university of groningen

faculty of mathematics and natural sciences

Zernike Institute for Advanced Materials – Photophysics and Opto-Electronics

Controllable p-type doping of PbS colloidal quantum dots

Bachelor Thesis

Applied Physics

Klaas Isaac Bijlsma

Supervisors:

D.M. Balazs

prof. dr. M.A. Loi

Second examiner:

dr. L.J.A. Koster

Groningen, July 2016

Abstract

Colloidal quantum dots (CQDs) are very promising for future use in optoelectronic devices because of the tunability of the band gap and low-cost production techniques. Doping CQDs, which is a very important requirement for application in semiconductor devices, is however still challenging. In this bachelor research project the possibility of doping CQD thin films by altering the stoichiometry of the QDs is investigated. Field-effect transistors (FETs) with lead sulfide (PbS) CQDs as active layer were fabricated and sulfide ions were added to shift the QD stoichiometry. The two important graphical products of FET measurements, namely output and transfer curves, were compared for FETs treated with different amounts of sulfide. The intrinsic PbS QDs were found to exhibit ambipolar behaviour, with electrons being the dominant charge carrier. It was found that changing the stoichiometry towards more S-rich character gives rise to p-type doping, and eventually shifts the behaviour from semiconducting to metallic-like. The conductance of the device at zero gate voltage was increased by almost three orders of magnitude. The transition to the metallic state is estimated to occur at a S/Pb ratio of 1.3. This result is in line with predictions based on density functional theory (DFT) calculations reported in literature.

Contents

Chapter 1: Introduction

All modern electronics, including transistors in computer chips, solar cells and light emitting diodes (LEDs) in screens and lighting, are based on semiconductors. Semiconductors are materials with an energy gap between their valence band and conduction band, giving rise to interesting and useful behaviour. The vast majority of modern electronics are based on 'traditional semiconductors', such as bulk silicon and gallium arsenide. However, the production of devices with those traditional semiconductors requires high purity materials and expensive methods. In recent years, much research has been done on a new generation of semiconductors, for example colloidal quantum dots, organic semiconductors and carbon nanotubes. These materials all have in common that they are solution processable, leading to the promising picture of low-cost devices, produced by printing or coating of thin films [1].

Colloidal quantum dots (CQDs) are crystals of conventional semiconductors, consisting of only hundreds to a few thousand atoms. They have a typical size of 2 to 20 nm and are therefore also called nanocrystals (NCs). To illustrate, figure 1.1 shows a transmission electron microscope (TEM) image of a CdSe quantum dot. Because of the small size, the charge carriers become quantum confined, leading to discrete energy levels in the valence and conduction band. Moreover, the size of the band gap becomes dependent on the size of the QD [3]. It is this property that makes them particularly interesting for applications in solar cells and LEDs. Experimental observation of quantum confinement in small crystals was first reported in the 1980s [4]. Because of the many possible applications and the fact that CQDs are solution processable, they have gained a lot of attention in research in the last decades. Substantial progress has already been made in understanding their properties, synthesis, and the incorporation of individual CQDs into coupled quantum dot solids. However, still a lot of research is needed and done, especially at controlling the trap states in order to improve the conductivity of CQD solids, and at achieving controllable doping which is necessary for application in devices.

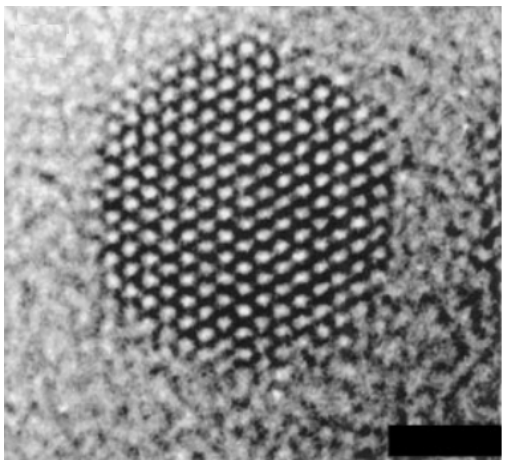

Figure 1.1: TEM image of a CdSe quantum dot. Scale bar = 1.5 nm. Source: [2]

A strong requirement in realizing semiconductor devices is the ability to control the doping of a semiconductor. This means that either electrons (n-type) or holes (p-type) are made the dominant charge carrier. This can be achieved by permanently shifting the Fermi energy E_F towards the conduction band or valence band, respectively. In traditional semiconductors, doping is usually done

by adding a small amount of impurity atoms having a different valence, which directly adds one type of charge carrier. There are certain factors that cause the controlled doping of CQDs to be more challenging. The traditional method of adding heterovalent impurities is difficult in CQDs, because of thermodynamic reasons. Synthesizing a nanocrystal with impurities is energetically not favourable, since the impurities destabilize the structure. Besides, a single heterovalent atom per quantum dot implies a doping concentration of 10^{-3}, or 10^{19} cm^{-3}, which is considered extremely heavy doping in a bulk semiconductor [5].

Due to the small size and the synthesis method, the stoichiometry is deemed to be different from what it would be in bulk, e.g. there usually are more Pb atoms than S atoms in PbS CQDs, while in bulk their ratio would be one. The uncoordinated surface atoms lead to dangling bonds which cause states in the band gap of the CQDs. Consequently, the band structure and the position of the Fermi-level will depend on the stoichiometry and the surface quality [6]. However, because of this, changing the stoichiometry can also be a method of doping CQDs.

The aim of this bachelor research project is to investigate the possibility of doping CQDs by acting on the surface of the QDs when they are assembled in thin films. In particular, lead sulfide (PbS) CQDs are studied by fabricating field effect transistors (FETs). The stoichiometry is then changed towards more S-rich character by adding sulfide ions to the PbS CQDs. The two important graphical products of FET measurements, namely output and transfer curves, are compared for FETs treated with different amounts of sulfide. It is found that adding sulfide ions to the QDs indeed gives rise to p-doping and eventually shifts the behaviour from semiconducting to metallic-like. This transition is found to occur at a S/Pb ratio of 1.3, which agrees with predictions made in literature. The transition is also seen in the conductance, which is increased by almost three orders of magnitude.

Chapter 2: Background

2.1 Physics of quantum dots

When the Schrödinger equation is solved for an electron in a spherical cavity of radius R, with zero potential energy inside and infinite outside, one obtains the following expression for the energy levels [7]:

$$E_n = \frac{n^2 h^2}{8 m_e R^2} \tag{2.1}$$

The separation between two adjacent energy levels is

$$E_{n+1} - E_n = (2n+1)\frac{h^2}{8 m_e R^2} \tag{2.2}$$

In the case of a bulk sphere, R is very large and the different energy levels merge into a continuum of states. If R is small however, such as in a quantum dot, the energy levels are discrete with forbidden energies in between them. This phenomenon is called quantum confinement. Conceptually, one can think of the electron in the (very large) bulk sphere as being essentially a free particle, but in the (small) quantum dot the electron 'feels' the walls and is confined. The same effect happens with electrons inside atoms, therefore QDs are also called 'artificial atoms'. The electron, hole and exciton, which is a quasi-particle of an electrostatically bound electron-hole pair, are quantum confined if the size of the nanocrystal is smaller than the Bohr radius of the exciton [8]. Quantum confinement in QDs can be observed as peeks in absorption spectra. Important transitions between discrete energy levels are responsible for increased absorption of certain photons of energy corresponding to these transitions. The $1/R^2$ dependence of the simplified model is important, because it shows that the band gap of semiconductor QDs is size-dependent. This can nicely be seen in figure 2.1, which shows the absorption spectra of CdSe quantum dots of diameter 2.8, 4.1 and 5.6 nm. It can be seen that the most prominent peak, which is due to the exciton and corresponds to the band gap, shifts to smaller wavelengths (higher energies) for smaller quantum dots. The size-dependence of the band gap opens the interesting possibility of band gap tuning, having many possible applications in photovoltaic cells and light emitting devices. For example, the efficiency of solar cells can be improved by tuning the band gap towards the optimum of 1.3 eV according to the Shockley-Queisser limit [10]. Another application

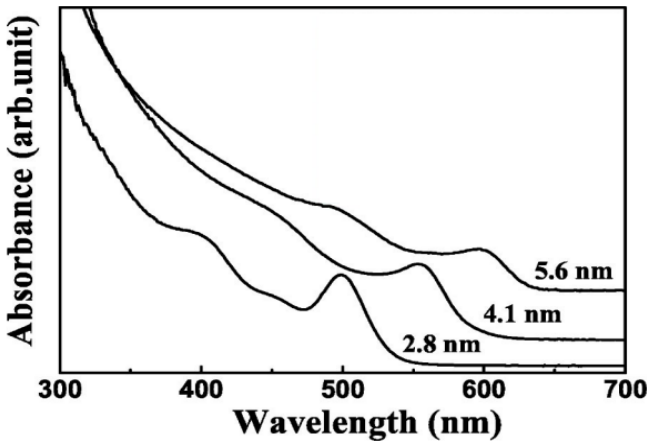

Figure 2.1: Optical absorption spectra for CdSe quantum dots of diameter 2.8, 4.1 and 5.6 nm. Source: [9].

in solar cells is incorporating different quantum dots with different band gaps into a tandem or multi-junction solar cell. This could lead to absorption of a broader range of the solar spectrum and therefore to higher efficiency solar cells [11]. QDs can also be used in biomedical applications, for example as fluorescent biological labels. The narrow tunable emission spectrum is favourable for multicolour labelling diagnostics [12]. Also metallic and magnetic QDs can be synthesized, with mainly biomedical applications [1]. In this thesis only QDs based on semiconductors are considered because they have properties which are interesting for optoelectronics.

2.2 Synthesis of colloidal quantum dots

Quantum dots are usually synthesized using the hot injection method [13]. This results in a colloidal solution of QDs and they are therefore called colloidal quantum dots. The hot injection method involves the rapid injection of a cold solution of one of the precursors needed for the formation of the QD into a high-temperature mixture of the other precursor and long organic molecules called *ligands*. This causes immediate nucleation, but since the concentration of precursor and temperature drops, nucleation stops after a certain time. Then the semiconductor crystals start to grow. The temperature and duration of the growth phase determine the size of the QDs. The ligands bind to the surface and prevent further growth. Moreover, the ligands make it possible to have a stable dispersion of CQDs in either aqueous or organic solvents. Figure 2.2 shows the structure of a PbS QD with oleic acid ($C_{17}H_{33}COOH$) ligands, obtained from a simulation.

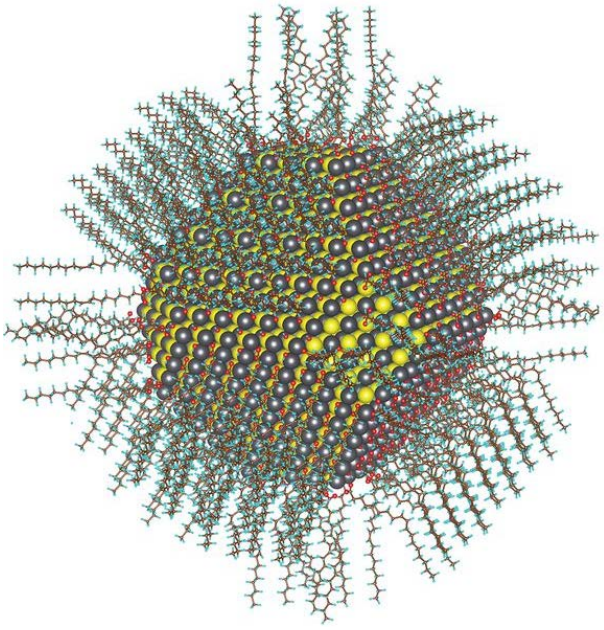

Figure 2.2: Calculated atomic structure of a 5 nm PbS cQD passivated with oleic acid. Colours: gray: Pb, yellow: S, red: O, brown: C, blue: H. Source: [14].

Group II-VI (CdS, CdSe, CdTe) materials were the first to be synthesized into QD form. Later also group III-V (InP, GaAs) and group IV-VI (PbS, PbSe) semiconductors became popular semiconducting materials for QDs [15]. Later adaptations of the hot injection method made it possible to synthesize CQDs with shapes different from spheres, such as cubes and multipods [16]. The stability and performance can be improved by growing a shell of a wider-bandgap semiconductor around the nanocrystals, yielding so-called core-shell quantum dots [13].

2.3 Solids of coupled quantum dots

A thin film of CQDs can be formed by evaporation of the solvent on a solid surface. The final order of the crystals depends on the solvent evaporation time and the interaction between the QDs [15]. Common techniques for making QD thin films are spin-, spray- or dip-coating and doctor blading.

The long ligands lead to relatively large separation between the dots, causing the charge transport between the QDs to occur via 'hopping', if it occurs at all. The conductivity can be increased if the distance between the QDs is decreased. Then the individual wavefunctions overlap more and the discrete energy levels form bands of electronic states. This effect is partly due to the Pauli exclusion principle, and is similar to the behaviour of atoms in a crystal, i.e. the coupling between the atoms increases as the interatomic distance decreases. Figure 2.3a shows this process schematically. In a process called *ligand exchange*, the original ligands are replaced with shorter ones, thereby reducing the inderdot separation. The ligands can be either organic or inorganic molecules, with the same charge as the original ligand. Examples are alkyl thiolates, amines and acids or halometallates, halides and pseudohalides [15]. Usually this is done after deposition of the CQD solid. A downside of this so-called solid exchange is that voids and cracks can appear due to the reorganisation of the QDs. This can be repaired by depositing a new layer after exchange of the previous one, although the order may be of lower quality [15].

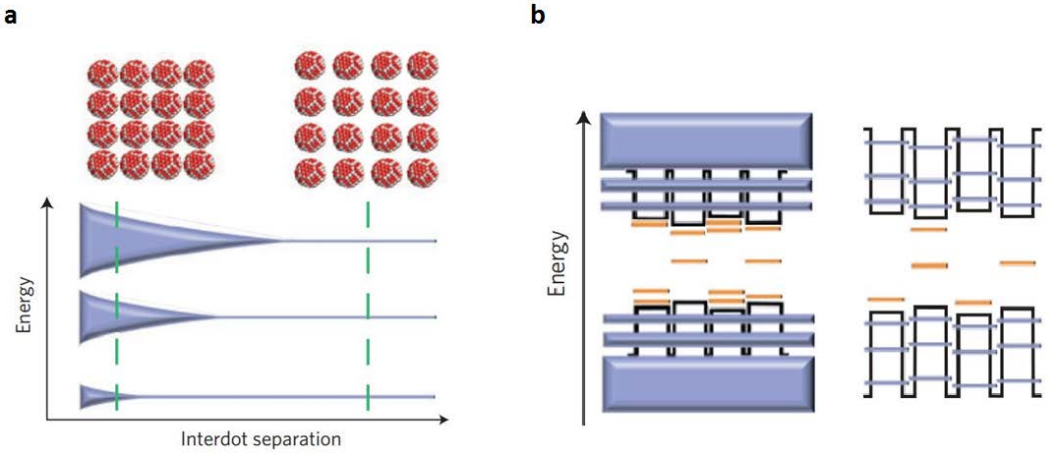

Figure 2.3: Electronic structure of QD solids. a) Effect of ligand exchange. b) Formation of minibands in a QD solid and the effect of disorder on uncoupled QDs. Source: [15].

The right hand side of figure 2.3b shows the electronic structure of the individual QDs forming the solid. Due to the relatively large surface area of the QDs and the fact that surface atoms are not fully coordinated, there are a lot of dangling bonds where other atoms and molecules can easily attach to, causing trap states that lie within the band gap. Quantum dots synthesized in the same batch usually have a standard deviation in size of about 5%. This effect causes a certain distribution in discrete energy levels. When looking at the QD solid, there may not have been enough time to rearrange, or the ligand exchange may not be fully completed, leading to differences in the interdot separation and therefore in the barriers seen by QDs. The energetic disorder acts against band formation. Band formation requires a bandwidth from exchange coupling larger than the energy detuning of states, the natural line widths of the states and larger than the charging energy caused by electron-electron repulsion in small dots [17]. Ideally, the resulting energy diagram for coupled QDs consists of broadened minibands forming a valence and conduction band, with defect states in the band gap, as can be seen in the left hand side of figure 2.3b. Because of the disorder however, it is unlikely that CQDs exhibit real band-like transport, but the conductivity and mobility can certainly be improved [17].

2.4 Stoichiometry based doping

As already discussed in the introduction, controlled doping of CQDs is difficult, because the crystals are intrinsically off-stoichiometric and synthesizing them with impurities is thermodynamically unfavourable. Nevertheless, there are some methods that have shown to be effective in doping CQDs [6]. The first is doping through oxidation: both adsorbed molecular oxygen as well as (hydr)oxide anions reacting with the surface of lead chalcogenide CQDs give rise to p-doping. Because the NCs are so small, they have a relatively large surface, making this effect significant. A second method is doping through ligand control, for example, hydrazine has shown to give n-type doping. Ligands also passivate the surface, and can prevent oxidation, thus influencing the doping. Other methods are doping by adding aliovalent impurities and remote doping [6]. The approach of the current research is stoichiometry based doping.

Stoichiometry describes the ratio of anions to cations. In a paper by the J.C. Grossman group, the impact of stoichiometry on the electronic structure of PbS quantum dots is investigated using *ab initio* density functional theory (DFT) calculations [18]. Figure 2.4 shows their calculated projected density of states (PDOS) as a function of energy relative to the Fermi energy. Figure 2.4a shows the density of states of a cubic $Pb_{108}S_{108}$ QD, i.e. a QD of perfect stoichiometry. It can be seen that the S atoms are mainly responsible for the states in the valence band and the states in the conduction band arise mainly from Pb atoms. This can be explained by the fact that S atoms have a higher ionization potential than Pb atoms. Figure 2.4b, which belongs to a cubic QD with one more Pb atom than S atoms, shows that a mid-gap trap state close to the conduction band edge has appeared.

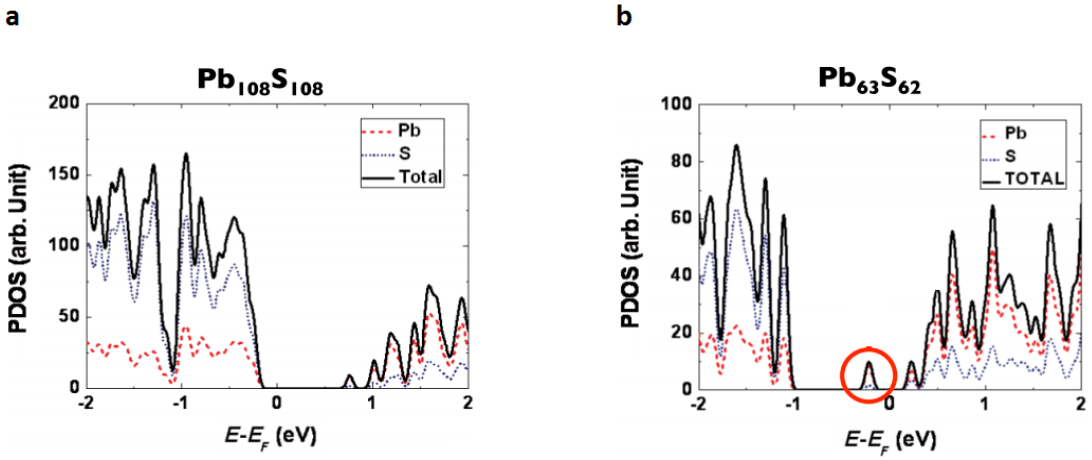

Figure 2.4: PDOS as a function of energy. a) For a perfect stoichiometric PbS QD. b) For a just off stoichiometric PbS QD. Encircled in red is a mid-gap state. Source: [18].

Figure 2.5 shows calculated Kohn-Sham energy levels for QDs with a range of different stoichiometries. The more off-stoichiometry QDs are obtained by modelling {1 1 1}-faceted QDs. Starting from a perfect semiconductor at a S/Pb ratio of 1, if the QD becomes more S-rich, more states delocalized over S atoms appear around the Fermi level, which is shifted downwards. Increasing further the S-atom content, the electrical behaviour changes from semiconducting to metallic. A similar effect occurs when the QD becomes more Pb-rich, with more states delocalized over Pb atoms appearing and a Fermi level of higher energy (closer to the conduction band).

The interpretations of both figures suggest that changing the stoichiometry such that they are S-rich is a possible way to p-dope PbS CQDs.

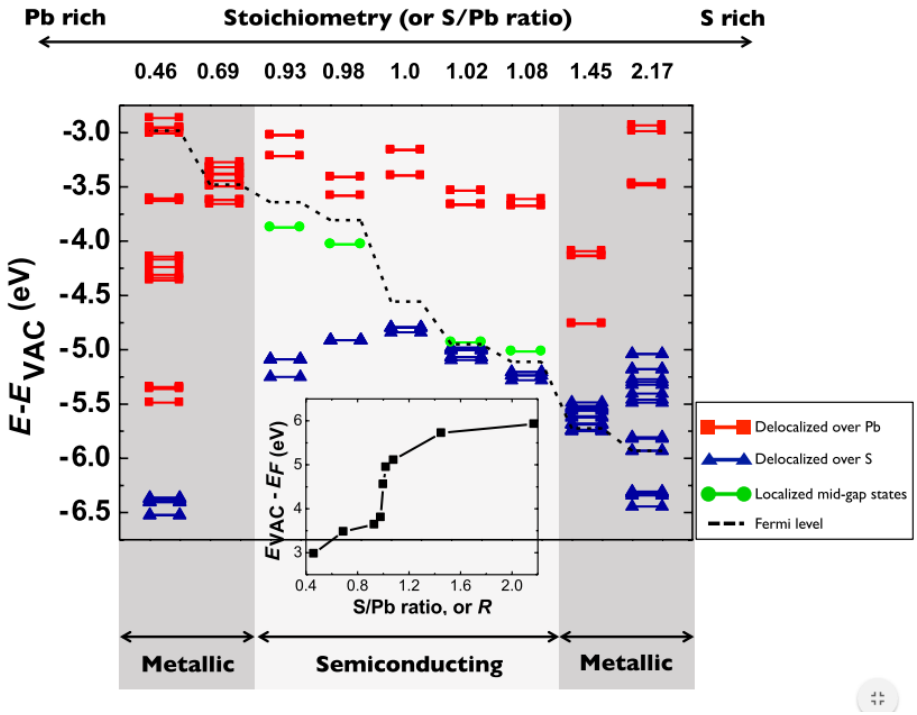

Figure 2.5: Kohn-Sham energy levels for QDs with a range of different stoichiometry. The inset describes E_{vac} -E_F as a function of QD stoichiometry. Source: [18].

2.5 Field-effect transistors

Field-effect transistors (FETs) are three-terminal devices in which the conductivity of a semiconducting channel depends on a voltage applied to the gate. It can act as a logical element because the signal between two terminals depends on the state of the third. In FETs based on 'traditional' semiconductors, either electrons or holes are the charge carriers, depending on the doping. Such devices are called unipolar FETs. On the other hand, when both electrons and holes can simultaneously be mobile inside the semiconducting channel, one speaks of ambipolar FETs. This could give the opportunity to develop more compact complementary metal-oxide semiconductor (CMOS) devices [19]. Nowadays these are made by combining a separate n- and p-type device. In the following paragraphs the working principles of ambipolar FETs will be explained, as well as two important type of graphs, namely output curves and transfer curves [20].

Figure 2.6 shows the basic structure of a FET. Between a source and drain electrode is a semiconducting channel of width W and length L. An insulator separates the semiconductor from a third electrode, the gate. The source is usually held at ground ($V_s = 0$) and voltages are applied to the gate (V_g) and the drain ($V_d = V_{ds}$). Depending on the combination of those voltages, electrons and/or holes will be accumulated at the semiconductor/insulator interface and a current I_d will flow between the source and drain electrodes.

First, we consider the case when V_{ds} is zero. When a positive V_g is applied, electrons are induced in the semiconducting channel, coming from the electrodes. The first induced electrons fill up the trap states in the band gap and hence cannot carry current. Only after a certain threshold voltage $V_{th,e}$ mobile electrons are induced. With the same reasoning it can be understood that mobile holes are accumulated after applying a V_g more negative than a hole threshold voltage $V_{th,h}$.

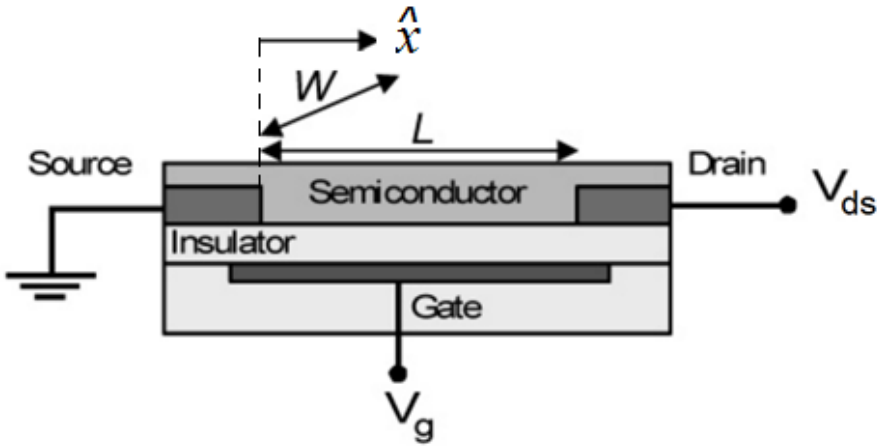

Figure 2.6: Schematic of a field-effect transistor. Source: [20].

Now let's assume that a fixed positive gate voltage $V_g > V_{th,e}$ is applied, so we are (initially) in the electron accumulation mode, and the drain voltage is increased starting from zero. The voltage at a certain position along the channel varies linearly from $V(x = 0) = 0$ to $V(x = L) = V_{ds}$. For a small drain voltage ($V_{ds} \ll V_g$), the current increases linearly with drain voltage according to Ohm's law, this is the *linear regime*. As the drain voltage increases further, the potential difference between the gate and the drain also decreases further, and when $V_{ds} = V_g - V_{th,e}$, no electrons are accumulated at the drain anymore. This point is called the pinch-off point. Further increasing V_{ds} causes this point to shift to the left and a depletion region forms through which a space-charge limited saturation current can flow. In this *saturation regime* a constant electron current flows. Increasing the drain voltage even further makes the gate effectively negative. This causes holes to be accumulated if $V_g - V_{ds} < V_{th,h}$, and the current now increases again with V_{ds} because of an increase in the number of accumulated holes. Now both electrons and holes carry current, and this is called the ambipolar regime.

Figure 2.7a shows a typical output curve, i.e. the drain current versus the source-drain voltage, for an ambipolar transistor. The situation described above is shown in the first quadrant. Curve 4 nicely shows first the linear regime, then saturation and eventually an increasing current again due to holes. For lower (higher) gate voltages, the electron currents will be lower (higher), and the hole current will start at lower (higher) drain voltages. A similar process as described above happens when applying negative drain and gate voltages. First there will be a linear regime of hole current, then saturation and eventually the minority carriers (electrons) take over the current. This is shown in the third quadrant of figure 2.7a.

Another important type of graph is the transfer curve, in which the drain current is plotted as a function of the gate voltage. Usually the drain current is plotted on a logarithmic scale in order to be able to see behaviour over many orders of magnitude. In this way the curves have a V-shape, as can be seen in figure 2.7b. The left arm shows hole current (with possible minority electrons at very negative drain voltages) and the right arm showing electron current, separated by an off-current. For larger V_{ds}, the condition $V_g - V_{ds} < V_{th,h}$ for minority hole accumulation is satisfied for lower gate voltages already. This causes the off-current to increase in magnitude and move to more positive gate voltages.

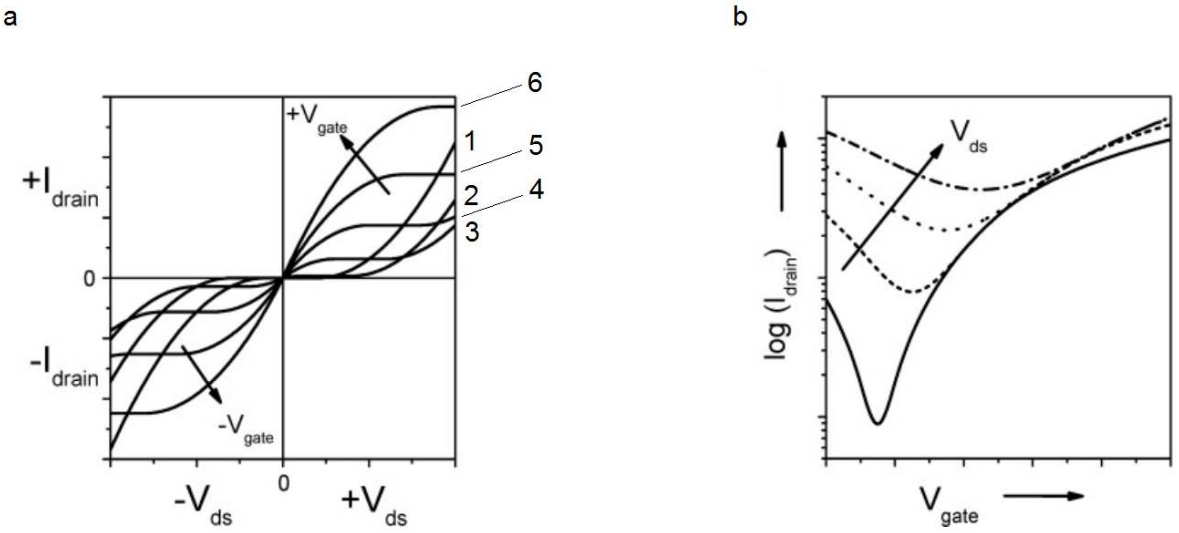

Figure 2.7: Calculated current-voltage characteristics for an ambipolar FET with equal hole and electron mobilities and slightly different threshold voltages. a) Output curves. In the first quadrant, V_g becomes more positive when going from curve 1 to 6, also indicated by the arrow. In the third quadrant, the arrow indicates the curves of more negative V_g. b) Transfer curves for positive gate voltages. The arrow indicates curves of more positive drain voltages. Adapted from: [20].

Now the equations for the drain current in the different regimes are derived [20], in order to obtain threshold voltages and mobilities. In the derivation, it is assumed that the number of accumulated charges inside the channel is determined by the field due to the gate voltage and not by the drain voltage. This so called gradual channel approximation is true for transistors with long channels, typically $L > 10d_{insulator}$. The total amount of mobile charge accumulated per unit area (Q_{mob}) as a function of position along the channel (x) is equal to

$$Q_{mob}(x) = -C\left(V_g - V_{th} - V(x)\right) \tag{2.3}$$

Here C is the capacitance per unit area of the insulator, V_{th} is either the electron or hole threshold voltage and $V(x)$ is the potential along the channel due to V_{ds}, varying linearly from $V(x=0)=0$ to $V(x=L)=V_{ds}$. The source-drain current I_d produced by the carriers is then given by

$$I_d = Q_{mob} v_x W \tag{2.4}$$

with v_x the velocity of the charge carriers in the x-direction and W the width of the channel. If we substitute $v_x = \mu E_x$ with μ the mobility of the charge carriers and E_x the electric field in the x-direction, and use $E_x = -dV(x)/dx$, we get

$$I_d dx = WC\mu\left(V_g - V_{th} - V(x)\right)dV \tag{2.5}$$

Assuming that the mobility is independent of voltage, this can be integrated to give:

$$I_d = \frac{W}{L} C\mu\left\{(V_g - V_{th})V_{ds} - \frac{1}{2}V_{ds}^2\right\} \tag{2.6}$$

Solving equation (2.6) for zero and keeping V_{ds} constant gives

$$V_{th} = V_g\big|_{I_d=0} - \frac{1}{2}V_{ds} \tag{2.7}$$

where $V_g\big|_{I_d=0}$ is the value of V_g for which I_d is zero. Therefore, in order to obtain the threshold voltage, one has to extrapolate the transfer curve to zero, and substract $\frac{1}{2}V_{ds}$ from the voltage intercept.

In the linear regime, where $V_{ds} \ll V_g$, equation (2.6) can be simplified to

$$I_d = \frac{W}{L} C \mu_{lin} (V_g - V_{th}) V_{ds} \tag{2.8}$$

As we saw earlier, in the linear regime the drain current is linearly proportional to V_{ds}, but also to V_g. According to equation (2.8), the field effect mobility in the linear regime can be obtained from the slope of the transfer curve:

$$\mu_{lin} = \frac{\partial I_d}{\partial V_g} \frac{L}{WCV_{ds}} \tag{2.9}$$

For drain voltages larger than $V_g - V_{th}$, the channel becomes pinched off and a saturation current flows. Therefore, equation (2.6) is no longer valid. An expression for this saturation current can be obtained by substituting $V_{ds} = V_g - V_{th}$ into equation (2.6), resulting in

$$I_{d,sat} = \frac{\mathrm{W}}{2\mathrm{L}} C \mu_{sat} (V_g - V_{th})^2 \tag{2.10}$$

It is clear that in the saturation regime, the square root of the saturation current is linearly proportional to the gate voltage.

Chapter 3: Materials

3.1 Lead sulfide nanocrystals

The PbS NCs used in the research were synthesized by the Functional Inorganic Materials Group at ETH Zurich, led by prof. dr. Maksym Kovalenko. They were synthesized by the hot injection method using oleic acid ($C_{17}H_{33}COOH$) as ligands. The particles were dissolved in anhydrous hexane at 57 mg/ml concentration. The CQDs from this batch were experimentally found to have their excitonic absorption peak at 1064 nm. This corresponds to a band gap of 1.17 eV, and using a sizing curve for PbS QDs made by Moreels et al. [21], they are estimated to have an average diameter of 3.5 nm.

3.2 Substrates

The electrical behaviour of the QDs was studied in FETs. The devices were fabricated by spin coating a thin layer of the CQD solution on a substrate, which already has the necessary components to function as a FET. A highly p-doped silicon wafer forms the bottom layer of the substrates. Besides functioning as bottom layer, it also functions as gate electrode. The insulating layer is thermally grown silicon oxide of 230 nm thickness. Gold electrodes (30 nm) are patterned using photolithography on top of 10 nm Ti to enhance to enhance the attachment. A single substrate has dimensions of 15x15 mm and contains four groups of four devices. The channel width W of all the devices is 10 mm, while the channel length L is different, namely 2.5, 5, 10 or 20 µm. Figure 3.1 shows a picture of a substrate with the 16 devices, indicating the different components on one device.

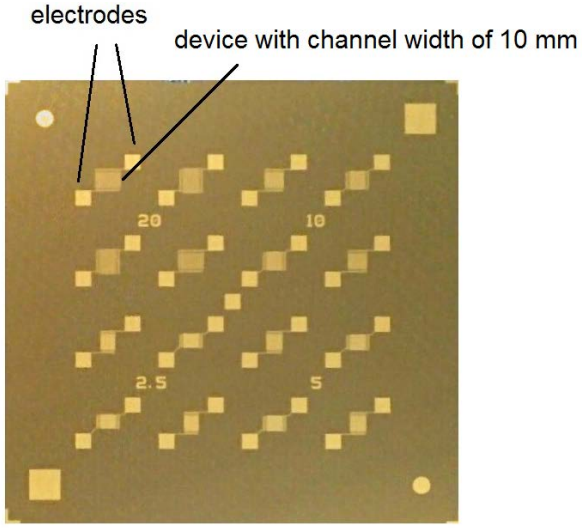

Figure 3.1: Picture of the substrates used, indicating the electrodes and channel of one device. The numbers (2.5, 5, 10 and 20) indicate the channel length of the four devices surrounding that number.

The capacitance per unit area of the insulator, introduced in equation (2.3) and needed to calculate the (linear) mobility in equation (2.9) can now be calculated according to the following equation:

$$C = \frac{\varepsilon_d \varepsilon_r}{d} \tag{3.1}$$

with ε_d the vacuum permittivity, ε_r the dielectric constant and d the thickness of the insulator. The dielectric constant for SiO_2 is 3.9, and together with a thickness of 230 nm this gives C = 150 µF/m^2.

3.3 Miscellaneous

Formamidinium iodide (FAI) was used for the ligand exchange (see figure 3.2). It is purchased from TCI Chemicals. To encapsulate the device and protect it against adsorption of other molecules, especially water and oxygen, a protective layer of a polymer was sometimes used. It is actually a terpolymer of vinylidene fluoride (VDF), trifluoroethylene (TrFE) and 1, 1-chlorofluoroethylene (CFE): p(VDF-TrFE-CFE). This polymer has a high dielectric constant of 50. All solvents that were used (hexane for the PbS nanocrystals, cyclohexanone for the polymer, and methanol for FAI, Na_2S and NaHS, are anhydrous and purchased from Sigma-Aldrich.

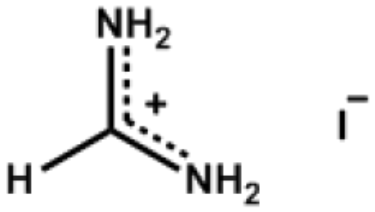

Figure 3.2: Structure of formamidinium iodide

Chapter 4: Experimental methods

This chapter describes how the experimental part of the research was performed. In short, the procedure consisted of cleaning the substrates, making solutions and then fabrication by spin coating. The devices properties were characterized with a FET probe station.

It is essential to work in a clean environment and minimize the amount of dust, since the FET channels have small dimensions. Dust particles or other contamination on the substrates can be catastrophic for good device operation. For this purpose, the experimental work was performed in a cleanroom. This cleanroom has no direct contact with other parts of the building, the air is filtered and the people working in it wear special anti-dust clothing. The cleanroom has an ISO 7 classification, meaning that a maximum of 352000 particles of size 0.5 μm and larger is present per cubic metre. Furthermore, the PbS QDs and some other materials, e.g. FAI, are very sensitive to oxidation. It has already been shown that oxidation causes p-doping of PbS QDs and the formation of electron-trap states [22]. To exclude the effect of (uncontrolled) doping by air and prevent deterioration of materials, the devices were fabricated and measured inside gloveboxes with a nitrogen atmosphere. In these gloveboxes the H_2O level is kept below 1 part-per-million (ppm), and the O_2 level is below 4 ppm. For the same reason, only anhydrous solvents were used.

4.1 Fabrication

4.1.1 Preparation

As a result of the photolithography process, the substrates are covered with a photoresist layer. This photoresist was removed by ultrasonic cleaning in acetone for 10 minutes. Afterwards the substrates were treated with ozone for 1 minute in a plasma chamber to remove any organic residues. Then another two ultrasonic cleaning steps of 10 minutes each followed, first in acetone and then in isopropanol. Finally, the samples were dried in an oven at 120°C for at least 20 minutes or overnight at 80°C to evaporate all the solvents. This part of the preparation was done on a so called wetstation in the cleanroom, which provides a constant laminar flow in order to minimize the chance of contamination even more. Just before fabrication the substrates were transferred into the glovebox. The solutions used for the spin coating were prepared inside the glovebox with anhydrous solvents. An analytical scale with accuracy 0.1 mg was used.

4.1.2 Spin coating

The thin films of QDs were made by spin coating the colloidal solution onto the substrate. In this technique a few droplets of a liquid are deposited onto the centre of a substrate, followed by the fast spinning of the substrate. A thin layer is formed by centrifugal forces causing the fluid to spread over, and eventually off the substrate, and also by evaporation of the solvent. The final thickness of the film depends both on the solution properties and on the chosen spinning parameters [23]. For example, a more viscous fluid will give a thicker layer, as will a solution of higher concentration. Important parameters that can be set are the rotational acceleration, final rotational speed and spinning time. Higher rotational speeds yield thinner films. The process can be performed with the lid open or closed: evaporation of the solvent is slower in the closed configuration due to vapour saturation in the limited volume.

The spinning was started immediately after deposition of the PbS solution, because the hexane is very volatile. Upon completion of this step, a few droplets of a 20mM FAI solution in methanol were applied

to the PbS CQD thin film and left to react for 30 seconds before the spinning was started. During this 30 seconds, the long oleate ligands are replaced with iodide ions, causing the interdot spacing to decrease and thereby the conductivity to increase. In order to get rid of the formamidinium ions a washing step was done, in which methanol was deposited and the spin coating was started after five seconds. From now one, the three previous steps together will be said to have formed one layer of PbS.

The next step of the fabrication was to act on the stoichiometry of the PbS QDs by adding sulfide ions in the form of a solution of sodium sulfide (Na_2S) or sodium hydrosulfide (NaHS) in methanol. This was done directly after the washing step was finished by adding 75 µl of the sulfide solution and waiting 30 seconds before starting the spinning. In this step the applied amount of liquid was precisely controlled (75 µl), since only then the behaviour of FETs treated with different concentrations of sulfide solution can be compared. After the sulfide treatment, again a washing step was done with methanol.

Based on existing experience in the group, spin coat parameter set *1* from Table 4.1 was used for all of the spin coating steps that have been described up until here.

Parameter set	*Rot. Acceleration (rpm/s)*	*Rot. Speed (rpm)*	*Spinning time (s)*	*Open/closed*
1	1000	1000	30	closed
2	1000	1000	90	closed
	1000	1000	40	open

Table 4.1: Values for the spin coating parameters of two 'parameter sets' used in the project.

Usually three to six samples were made during one experiment. After completing the last one, all the samples were annealed for 15 minutes at 120°C. The environmental conditions such as temperature and level of contamination but also the way of cleaning and fabrication are expected to be very similar for these devices. Therefore they can be compared to each other, but not necessarily to devices made on different days.

In some experiments, the devices were covered with a polymer layer to protect them against adsorption of impurities, especially water and oxygen. This involved the deposition of a solution of 50 mg/ml p(VDF-TrFE-CFE) in cyclohexanone on the substrate and spin coating with parameter set 2. Since the polymer is more viscous, first a longer spinning step was needed with the lid closed. Also, cyclohexanone has a high boiling point causing it to dry slower. For this, an extra step was needed in which the spin coater lid is open.

4.2 Measuring the device properties

The device properties were measured on a probe station. First, on a small area of the substrate the applied layers and the silicon oxide were scratched away with a silicon-carbide pen in order to make a connection for the gate. Three very sharp tips that can be controlled with micromanipulators were used to connect to the source, drain and gate electrodes. In the project, only devices with the largest channel length of 20 µm were measured. This is chosen because then the field produced by the source-drain voltage has as little influence on the charge distribution as possible, and because more charge carriers can be accumulated in longer channels. Of the four available devices, the device which looked the best regarding delamination and contamination was measured. In order to prevent leakage

current, the substrate was placed on a plastic plate, and the electrodes and channel area was separated from the rest of the substrate by scratching around with a steel blade. In this way, the (conducting) quantum dot layer is removed, and no current can flow across it. The voltages were applied and currents measured with an Agilent E5262A IV analyser equipped with two Source/Measure Units (SMUs) for the drain and gate voltage, the source was grounded. The applied voltages could be set by a computer, which also saved the corresponding measured currents in a text file. The output curves were obtained by varying V_{ds} from 0 to 60 V in steps of 1 V for fixed gate voltages of 0, 20, 40, 60 and 80 V for the n-channel. Negative drain and gate voltages of the same magnitude were applied for the p-channel. The transfer curves were obtained by varying V_g from -20 to 80 V in steps of 1 V for fixed drain voltages of 5 and 10 V (linear regime) and 40 V (saturation regime). Again, negative voltages were applied to record the p-channel. The mentioned range was scanned (forward scan), and then scanned backwards to the starting point (backward scan). Because PbS is a semiconducting material with high absorbance, the measurements were performed in dark. Figure 4.1 shows the effects on the measurements of measuring in dark and of scratching around the device. The meaning of the general shape will be explained later in the results, for now it can be seen that scratching causes the measured currents to be slightly larger. The effect may however sometimes be more significant. It can also be seen that measuring in dark is very important, since the currents are much higher and the shape changes for the measurement with lights on. This can be explained by the generation of extra charge carriers by absorbed photons.

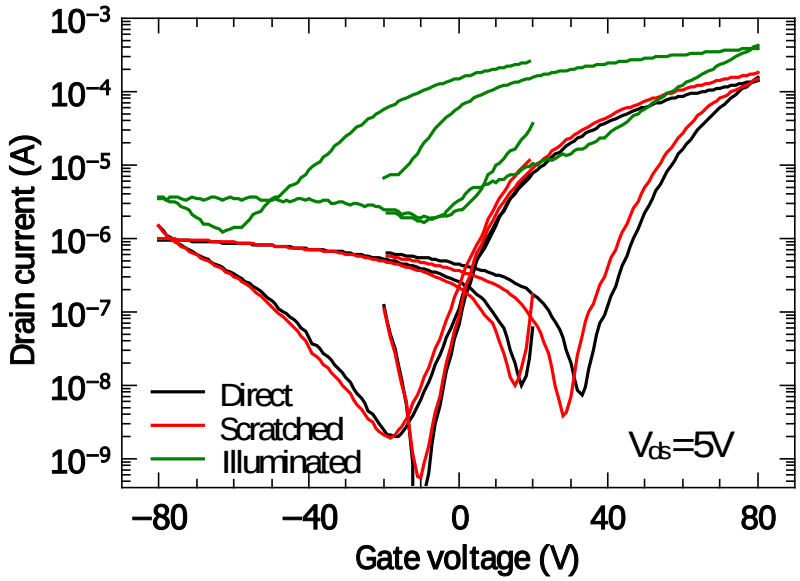

Figure 4.1: Transfer curves of an intrinsic PbS FET measured in dark (in black), in dark and scratched around device (in red) and with lights on (in green).

Chapter 5: Results and Discussion

5.1 Starting point: an intrinsic PbS CQD FET

In the first experiment of the project an intrinsic FET, i.e. without sulfide treatment, was made according to the procedure described in section 4.1. Based on previous experience in the group, the device was made with two layers: the first with 5 mg/ml PbS, the second with 10 mg/ml PbS. In this way, a relatively thick semiconducting channel forms, such that the electrical behaviour is independent of the thickness and the currents are high compared to the measurement noise. As said before, making a layer also includes ligand exchange with FAI and washing with methanol. The device was completed with a protective polymer layer, as described in section 4.1.

Figure 5.1 shows the output (I_d-V_d) and transfer (I_d-V_g) characteristics of this transistor. The linear and saturation regime is clearly visible for the n-channel output curves. The gate voltage dependence is as expected, namely a larger range of linear regime and higher saturation current for higher gate voltages. For the p-channel, a small hole current is seen, but eventually the minority carriers (electrons) take over the current. For more negative gate voltages, the hole currents increase and the electron current starts at more negative drain voltages. An important observation is that the hole currents are more than two orders of magnitude smaller than the electron currents. A small amount of hysteresis is seen. Also on the transfer curves it is seen that electrons are the dominant charge carriers. Still, ambipolar behaviour is clearly visible. This electron dominance can be explained by the fact that the intrinsic PbS QDs are Pb-rich. This stoichiometry situation gives rise to n-type doping, for the same reason as why p-type doping is expected for S-rich QDs. This intrinsic n-type character is unavoidable, since the oleic acid molecules bind to Pb atoms during synthesis, causing the outer shell to be Pb-rich. The mobilities are calculated according to equation (2.9) for the forward scan in the linear regime resulting in $\mu_e = 9.7 * 10^{-2}$ cm²/Vs and $\mu_h = 3.4 * 10^{-4}$ cm²/Vs. The on/off ratio is found to be 10^2 for holes and $4 * 10^5$ for electrons. A large amount of hysteresis is seen, indicating the presence of many trap states at the dielectric interface and the QD surface.

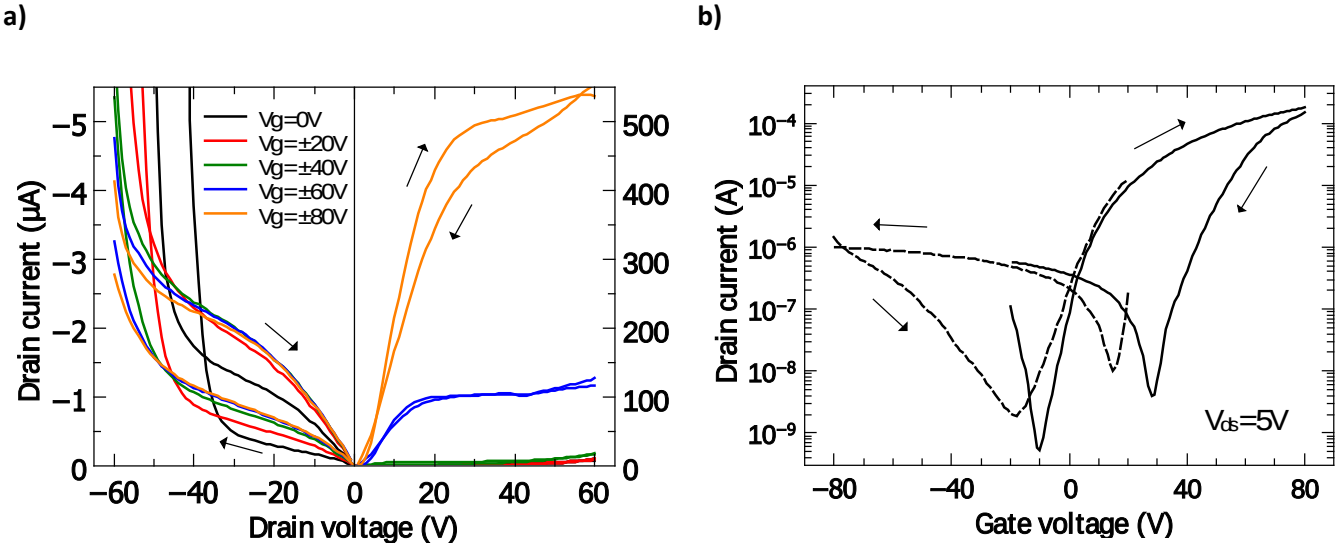

Figure 5.1: Intrinsic FET a) Output characteristics with p-channel (negative gate and drain voltages) on the left and n-channel (positive gate and drain voltages) on the right. Both the forward and backward scan are plotted, with the arrows indicating the direction of scanning. Note that the scale of the axes is different. b) Transfer characteristics of both n-channel (solid) and p-channel (dotted) in the linear regime. Again, the arrows indicate the direction of scanning.

5.2 Doping by Na_2S treatment and the influence of p(VDF-TrFE-CFE) on stability of the devices

In the previous section it was found that electrons are the dominant charge carrier in intrinsic PbS CQDs. As discussed in section 2.4, a way to p-dope the PbS NCs seems to be changing their stoichiometry towards more S-rich character. This is because the S atoms are mainly responsible for states in the valence band, and DFT calculations have shown that changing the stoichiometry such that the NCs become more S-rich shifts the Fermi level downwards and results in the formation of more states in that energy range. The first attempts to accomplish this involved treating the PbS layer with a solution of sodium sulfide (Na_2S) in methanol. In order to control the amount of sulfide introduced, precisely 75 µl solution of different sulfide concentration was deposited each time on a sample.

Several experiments were done, in which several sets of samples were made according to the description in section 4.1, each sample treated with a different concentration of Na_2S. The samples were covered with a layer of p(VDF-TrFE-CFE). Figure 5.2 shows the transfer curves of one of the experiments. The two devices treated with $3.16 * 10^{-5}$ M and 10^{-4} M Na_2S show ambipolar semiconducting behaviour, with the latter having a slightly smaller electron current and larger hole current. Moreover, a small positive shift in the onset voltage is seen. Both observations are indications of p-type doping. For the concentration of 10^{-3} M, the behaviour has changed drastically: the off-state has disappeared, and a large current with minimal gate voltage dependence is seen. This indicates metallic-like behaviour, meaning that the Fermi level is now inside the valence band.

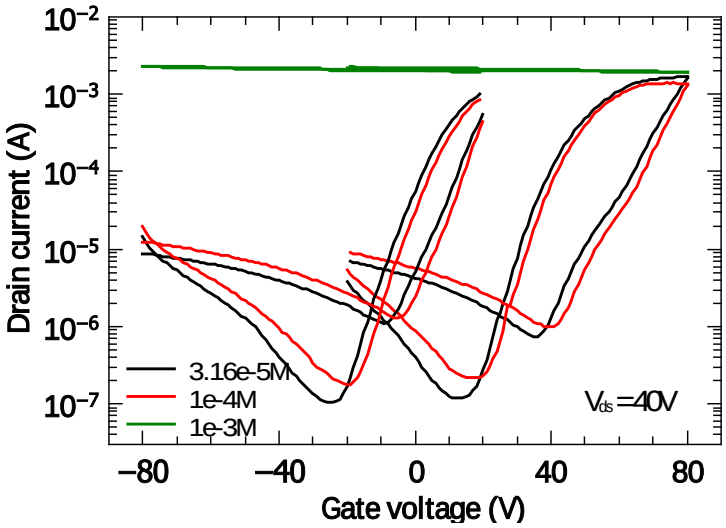

Figure 5.2: Transfer curves of 2-layered 5 and 10 mg/ml PbS FET, treated with 75 µl Na_2S solution in methanol, of concentration $3.16 * 10^{-5}$ M, 10^{-4} M and 10^{-3} M.

These results show that adding sulfur atoms to the PbS QDs indeed gives rise to p-type doping. However, three problems appeared during the first experiments. The first is that depositing the Na_2S solution caused delamination of the PbS layer. This happened especially with concentrations higher than 10^{-4} M on the 10 mg/ml PbS layer. The delamination was then so intense that large areas became uncovered and the active device area decreased substantially. Hence the measurements were unreliable, since the devices were not equally covered (the active channel area differed) and could not be compared to each other. Besides, some devices were damaged so much that no meaningful data could be collected. Figure 5.3 shows microscope images of a device with heavy delamination. There are two possible explanations for the delamination. The first is Coulombic repulsion of charged QDs. If

a) b)

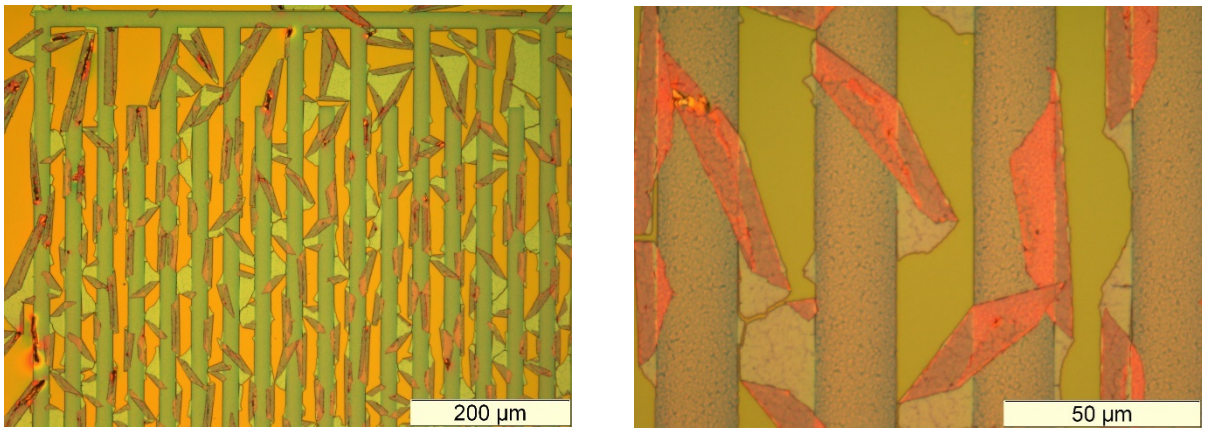

Figure 5.3: Microscope images of 2-layered 5 and 10 mg/ml PbS FET, treated with 75 µl 10^{-3} M Na_2S solution in methanol and a protective polymer layer. a) 10 times magnification b) 50 times magnification

the concentration of the sulfide solution is increased, more and more of the iodide ions will be replaced by sulfide ions. Eventually all of them are replaced and extra sulfide ions are added. In this way, the QD becomes more and more negatively charged, and the ordered lattice of QDs will break up. Another possible mechanism for the delamination is that the layer peels off because of an inhomogeneous vertical strain distribution in the layer. It is seen that the layers shrink while the sulfide ions replace the iodide ions. This may stem from the fact that in this second ligand exchange, the dots have a new possibility to reorganise themselves. If the layer is relatively thick, then this process may occur mainly at the top part of the QD layer. This causes the top part of the layer to contract more than the bottom part, causing the layer to break up.

A second problem is that the transport properties changed over time. Figure 5.4 shows the transfer curve of a device measured on the day of fabrication together with the curve of a measurement on the same device made 24 hours later. It can immediately be seen that the curves differ substantially. The electron current increases with almost a factor 2, the onset voltage shifts significantly to the left and the hole current decreases slightly. In short, the p-type doping is counteracted by significant n-type doping.

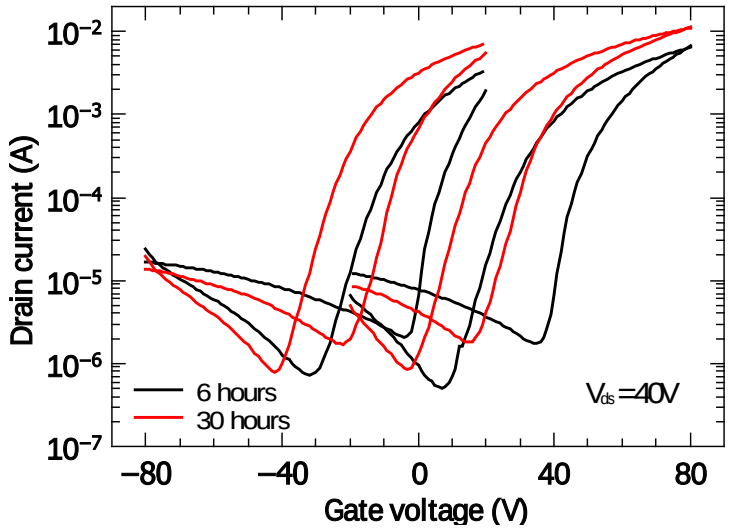

Figure 5.4: Transfer curve of 2-layered 5 and 10 mg/ml PbS FET, treated with 75 µl $3.16 * 10^{-5}$ M Na_2S solution in methanol and a protective polymer layer. The black curve is measured 6 hours after fabrication, the red curve 30 hours after.

Since the goal of the research was to investigate (p-type) doping, it was necessary to have a fabrication and measuring method that is stable in time regarding doping. Otherwise the applied variations are not the only cause of changes in observed behaviour, and no reliable conclusions can be made. This was also the reason for using the polymer layer: to protect the devices from p-type doping due to trace amounts of water and oxygen, which are unavoidably present inside the glovebox. It has already been shown that lead chalcogenides are easily oxidized [22], and low exposure to oxygen gives (reversible) changes due to adsorption of oxygen [24]. What was observed here however, is that the devices become more n-type during storage in the glovebox, which is undesirable for the same reason. A possible explanation is that the polymer layer dries very slowly and the cyclohexanone solvent interacts with the QD layer. In order to stop this process, the samples were annealed for 30 minutes at 95°C after coating with the polymer. Figure 5.5 shows the transfer curve of a device made according to this procedure, measured after 1 day and after 8 days. It can be seen that this results in a more steady behaviour, but still considerable n-type doping is seen.

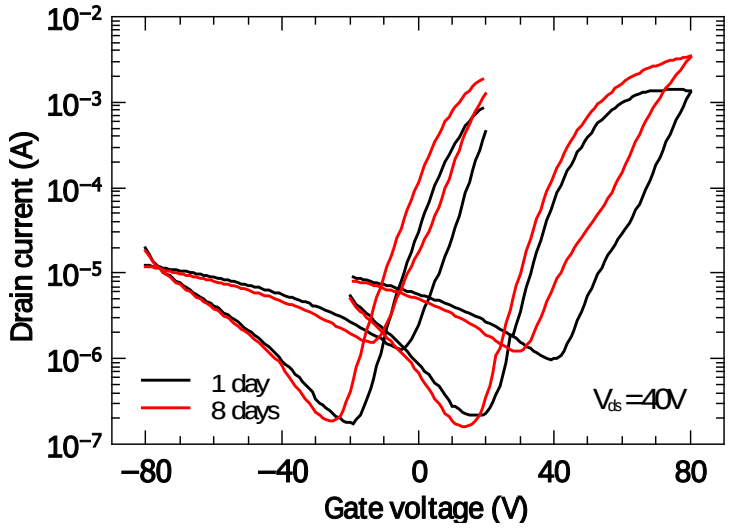

Figure 5.5: Transfer curve of 2-layered 5 and 10 mg/ml PbS FET, treated with 75 µl 10^{-4} M Na_2S solution in methanol. After applying a protective polymer layer, the device is annealed for 30 minutes at 95°C. The black curve is measured 1 day after fabrication, the red curve 8 days after.

Because the polymer layer seems to create a time-dependent effect on the properties of the QDs, it is not suitable as a protective layer. Instead, the devices were annealed for 20 minutes at 105°C right before the measurements in order to evaporate all of the adsorbed oxygen and water. It has already been demonstrated that annealing PbS CQD FETs that have been exposed to air gives almost full recovery of the original characteristics [25]. After annealing, the device was cooled for 20 minutes, such that the characteristics are measured at roomtemperature. To limit the amount of oxidation, the devices were always kept in nitrogen atmosphere between fabrication and measurement. Figure 5.6 shows a device that was made and measured according to this procedure, both measured after 1 day and after 7 days. It can be seen that the curves are very similar, especially when compared to figure 5.4 and figure 5.5. Still there are some small deviations, but these are acceptable. For the remainder of the project, this procedure was used to make and measure the devices.

The third problem involves the Na_2S solution. It was observed that a small amount of precipitate was present in the high concentration solutions. It is reported in literature that Na_2S dissolved in methanol partially reacts with methanol [26]. This fact made the experiments unreliable, since it was not known how much sulfide was applied exactly.

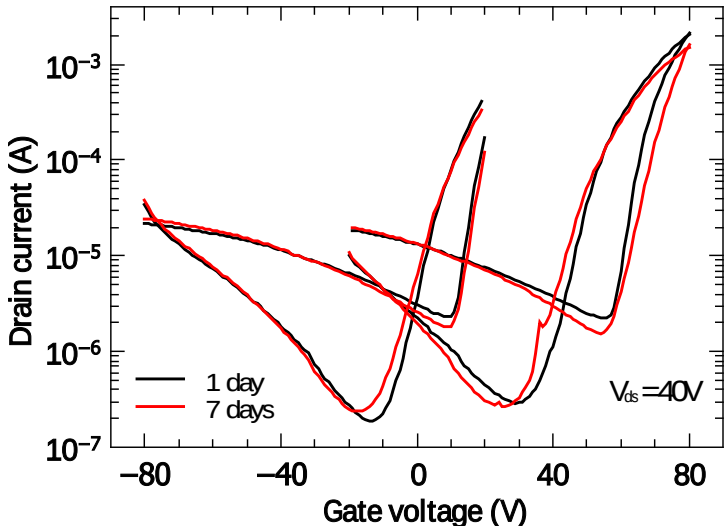

Figure 5.6: Transfer curve of 2-layered 5 and 10 mg/ml PbS FET, treated with 75 µl $2 * 10^{-4}$ *M* Na_2S *solution in methanol, without a protective polymer layer. The black curve is measured 1 day after fabrication, the red curve 7 days after.*

5.3 Doping by NaHS treatment

In order to try to decrease the amount of delamination, two layers of 5 mg/ml PbS were used such that the layer does not become too thick. A second change is that the PbS layer was treated with NaHS instead of Na_2S. The advantage of NaHS is that it is better soluble in methanol than Na_2S, making the concentration more reliable. Moreover, SH^- ions may charge the QDs less. With this method still some delamination was seen in the form of very fine grains, but the surface looked much smoother than in the previous part of the project. This can be seen by comparing Figure figure 5.7, which shows microscope images of a FET made with this method and also treated with a sulfide concentration of 10^{-3} M, with figure 5.3, prepared with the previous method. To further improve this method, one could make more layers of a lower concentration and do a ligand exchange after every layer. Another possibility to further decrease the amount of delamination is liquid ligand exchange. Solid ligand exchange is always a cause of cracks, since the volume lost in the process is not refilled with new QDs. To avoid this effect, solution-phase ligand exchange could be used. This involves the exchange of the long ligands with shorter ones before the spin coating process. To prevent the QDs to cluster together into a bigger crystal, more polar solvents are needed for electrostatic stabilization [15].

a) **b)**

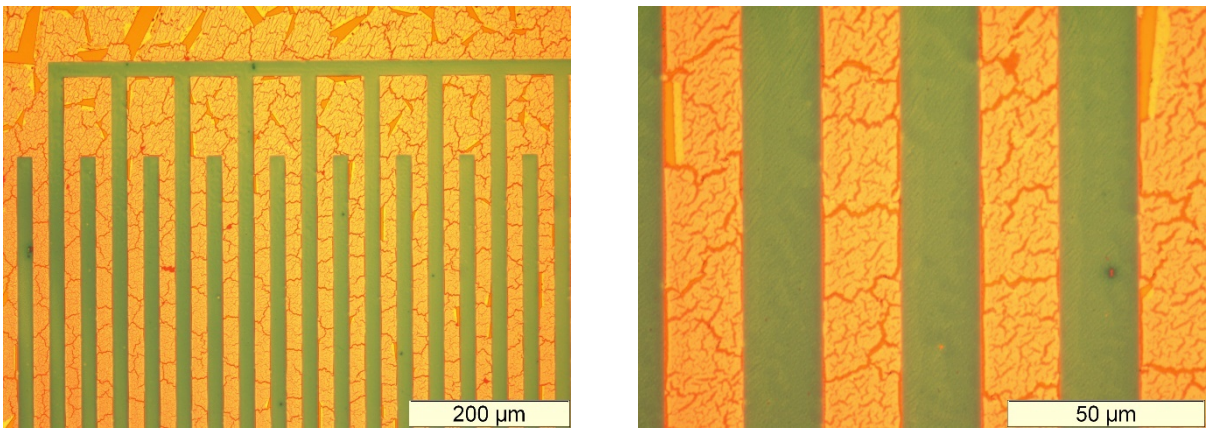

Figure 5.7: Microscope images of 2-layered 5 mg/ml PbS FET, treated with 75 µl 10^{-3} *M NaHS solution in methanol. a) 10 times magnification b) 50 times magnification*

A set of samples was fabricated with applied solutions of NaHS with concentrations varying from 10^{-5} M to 10^{-2} M. Figure 5.8 shows the transfer curves of these devices. At first, when the concentration is increased from 10^{-5} M to 10^{-4} M, the electron current decreases by almost 1 order of magnitude while the hole current decreases by less than a factor of 2. The decrease of hole current may be due to a difference in device quality, but it is less significant than the loss in electron current. Moreover, the onset voltage shifts towards more positive values. Both observations are indications of p-type doping. When the concentration is increased further to 10^{-3} M, a transition to metallic-like behaviour is seen. A concentration of 10^{-2}M shows higher currents and further decreased gate dependence.

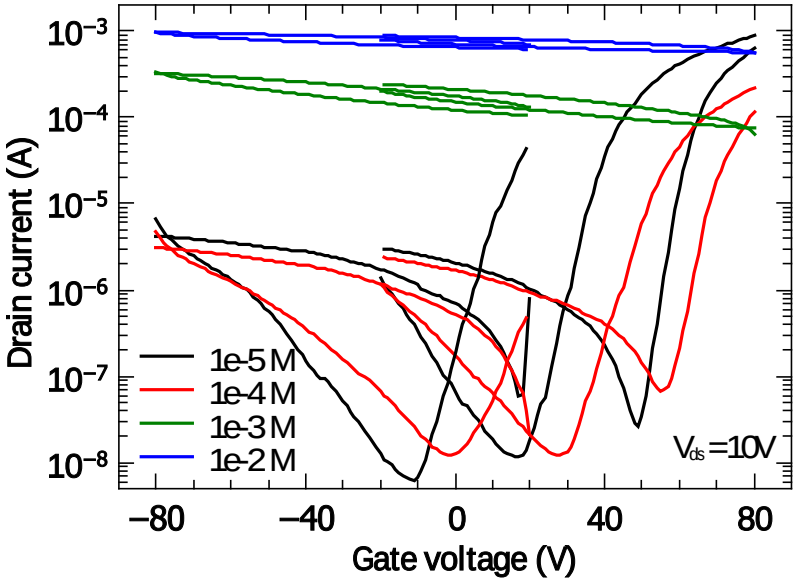

Figure 5.8: Transfer curves for 2-layered 5 mg/ml PbS FET, treated with 75 µl NaHS solution in methanol, varying in concentration from 10^{-5} M to 10^{-2} M.

The observations made above can be investigated further by looking at calculated threshold voltages, mobilities and conductance in table 5.1. The threshold voltages and mobilities are calculated with equations (2.7) and (2.9) respectively, which are only applicable for the devices showing semiconductive properties. The last column shows the conductance at zero gate voltage. Comparing the two devices showing semiconductive properties, both the electron and hole threshold voltage increase substantially when the sulfide concentration is increased. This means that electron accumulation is more difficult, while hole accumulation becomes easier. Both the electron and hole mobility decrease for increased concentration of NaHS, but the electron mobility decreases faster. The conductance decreases slightly initially, which may, again, be due to a bad device quality. The first device showing metallic behaviour, with 10^{-3} M sulfide applied, has a conductance of more than two orders of magnitude larger than the first devices. The device treated with the most sulfide has even a four times higher conductance than this first metallic device.

Concentration (M)	$V_{th,e}(V)$	$V_{th,h}(V)$	$\mu_e(cm^2/Vs)$	$\mu_h(cm^2/Vs)$	G (S)
10^{-5}	28.4	19.9	0.23	$6.4 * 10^{-4}$	$8.4 * 10^{-8}$
10^{-4}	41.9	24.2	0.068	$4.0 * 10^{-4}$	$5.8 * 10^{-8}$
10^{-3}	-	-	-	-	$1.7 * 10^{-5}$
10^{-2}	-	-	-	-	$7.2 * 10^{-5}$

Table 5.1: Threshold voltages, linear mobilities and conductance at zero gate voltage calculated from the transfer curves with $V_{ds} = 5\ V$. For the metallic curves, threshold voltages and mobilities cannot be calculated.

The change in behaviour can also nicely be seen in the output curves shown in figure 5.9. The device fabricated with 10^{-5} M NaHS (fig 5.9a), shows strongly electron-dominated semiconductive behaviour. When the concentration is increased to 10^{-4} M, in figure 5.9b, the electron current is suppressed by one order of magnitude. At the same time, there is a significant hole contribution in the n-channel at high drain voltages. In figure 5.9-c and -d, corresponding to 10^{-3} M and 10^{-2} M respectively, the linear and saturation regime is not present, ohmic behaviour is observed instead, indicating a transition to a metallic-like state. The last figure shows higher currents and lower gate dependence than the former. The general trend can be explained by a shift of the Fermi level from somewhere halfway in the band gap towards and into the valence band.

As a follow-up on the previous experiment, a new set of samples was made with concentrations varying between 10^{-4} M and 10^{-3} M. The resulting transfer curves are shown in figure 5.10. For $2 * 10^{-4}$ M, the off-state is still observed, but the off-current is increased considerably compared to the device without sulfide treatment (black line). Similar to the previous cases, the onset voltage is shifted to more positive voltages. For the next three higher concentrations, metallic behaviour is seen, with higher currents for higher concentrations.

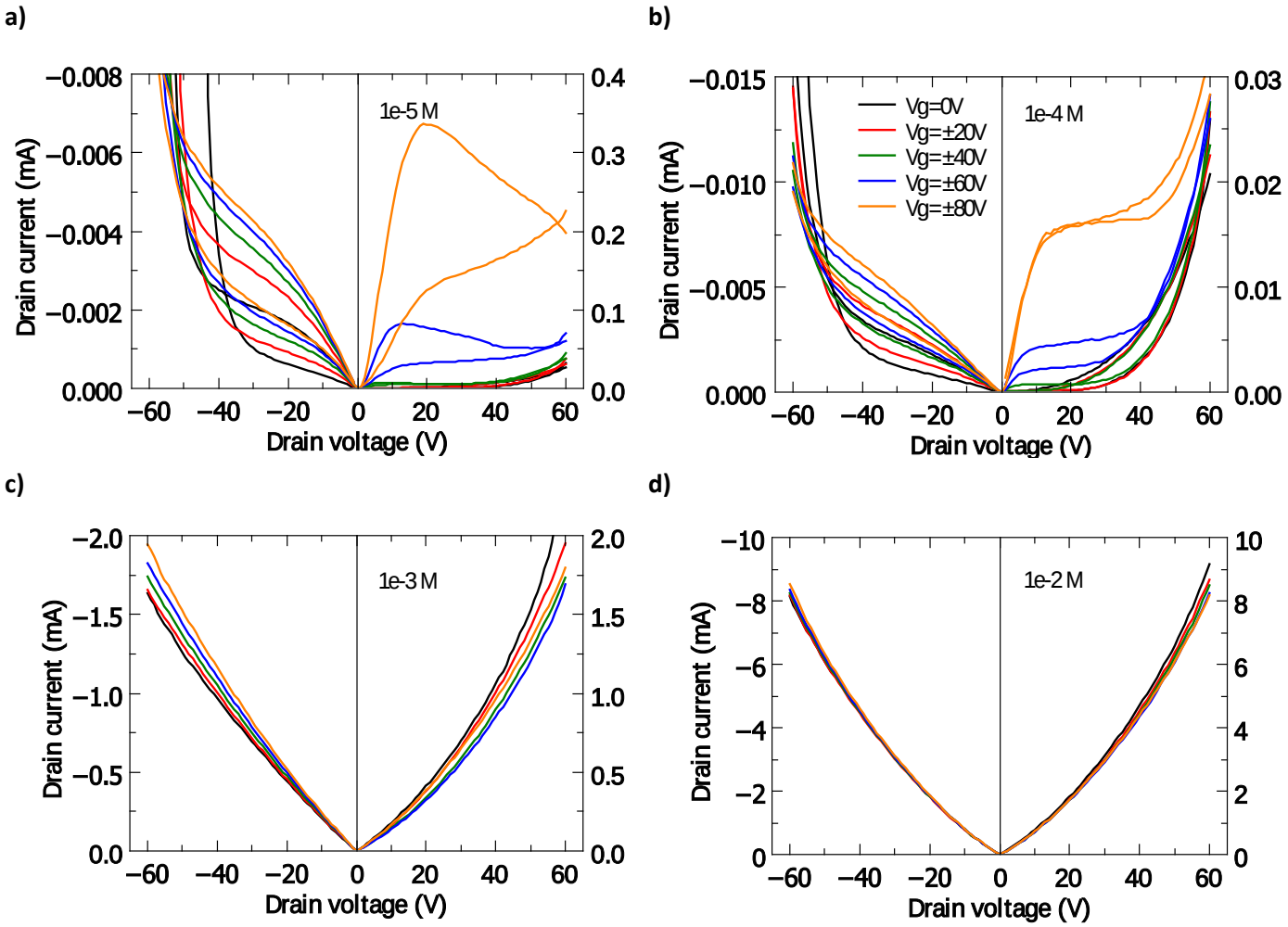

Figure 5.9: Output curves of the transistors made with 2 layers of 5mg/ml PbS and treated with 75 µl of different concentration NaHS in methanol. a) 10^{-5}M NaHS b) 10^{-4}M NaHS c)10^{-3}M NaHS d) 10^{-2}M NaHS. For clarity, only the forward scan is shown for c) and d) Note that the scale of the axes can be different for the n- and p-channel and per subfigure.

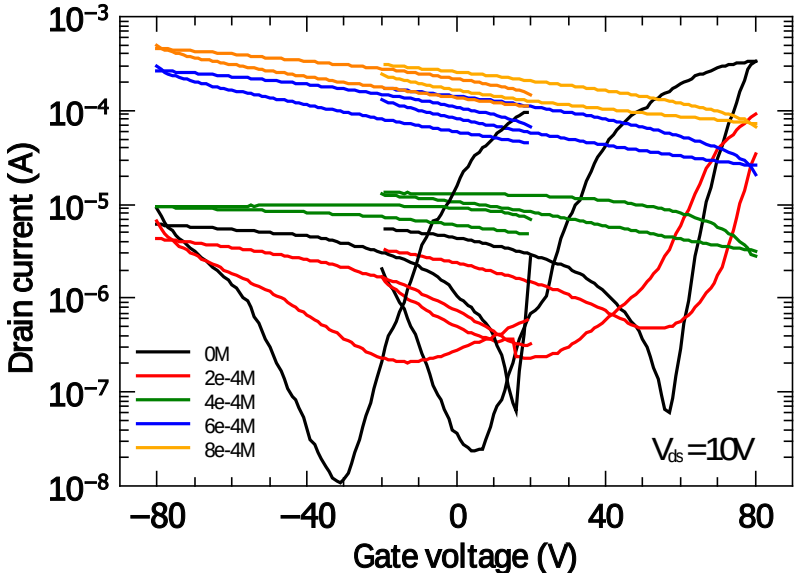

Figure 5.10: Transfer curves for 2-layered 5 mg/ml PbS FET, treated with 75 µl NaHS solution in methanol, of concentration between 10^{-4} M and 10^{-3} M, and one without.

It appears that the transition takes place around a concentration of $3 * 10^{-4}$ M. To estimate how many sulfide ions are added per QD to reach this transition, the thickness of the QD layer is needed. The thickness of the double layer is measured to be around 30 nm. Assuming that the whole volume of the QD layer is filled by a perfect super lattice of QDs with diameter 3.5 nm, one calculates $1.57 * 10^{14}$ QDs on the whole substrate. This is an upper limit; the actual value will be lower because of the cracks and imperfect ordering stemming from the ligand exchange. To improve this value and its uncertainty, STM images of the layer could be made, on which it can be seen how dense the QDs are packed on average. Because 75 µl of $3 * 10^{-4}$ M sulfide is applied two times, a total of $2.71 * 10^{16}$ sulfide ions are applied to the QDs, assuming that no sulfide is lost. The amount of sulfide added is also an upper limit, because a small volume may be left behind in the pipette and not all sulfide may attach to a QD. Combining these two values, one obtains that 172 sulfide ions are added per quantum dot. The fact that the two values are both an upper limit makes the value of 172 less unreliable, but it is not known to what extent a cancellation of overestimation occurs. A concentration of $2 * 10^{-4}$ M, which means 115 sulfide ions per QD, is certainly too low. On the other side, a concentration of $4 * 10^{-4}$ M , which corresponds to 230 sulfide ions per QD, is certainly too high. This factor therefore gives an uncertainty of less than 50 ions in the number of ions per QD.

In section 3.1, the diameter of the specific QDs used is estimated to be 3.5 nm. If the QDs are assumed to be a sphere of a perfect stoichiometric PbS rock salt lattice, the QD structure is estimated to be $Pb_{430}S_{430}$. In reality, the outer shell is formed by lead atoms and the QDs are therefore off-stoichiometric with an excess of lead. It is known that the S/Pb ratio is about 0.9, therefore the structure is estimated to be $Pb_{450}S_{410}$. Using these assumptions and the obtained 172 added sulfide ions, it can be concluded that the transition to metallic behaviour occurs at a S/Pb ratio of 1.3. This result is in line with the DFT calculations shown in figure 2.5, according to which the transition takes place at a S/Pb ratio between 1.08 and 1.45.

Conclusions and Prospects

In this bachelor research project the possibility of doping CQD thin films by altering the stoichiometry of the QDs was investigated. Field-effect transistors with lead sulfide CQDs as active layer were fabricated and sulfide ions were added to shift the QD stoichiometry. The two important graphical products of FET measurements, namely output and transfer curves, were compared for FETs treated with different amounts of sulfide.

The intrinsic PbS QDs were found to exhibit ambipolar behaviour, with electrons being the dominant charge carrier. An electron mobility of $9.7 * 10^{-2}$ cm^2/Vs was found, which is comparable to the best ones in literature.

In order to get the level of doping constant in time, the devices had to be protected against known p-type doping by adsorbed oxygen and water. For this purpose, the samples were encapsulated with a polymer layer of p(VDF-TrFE-CFE). It was found that this layer causes significant n-type doping over time, an effect that remains if the polymer layer is annealed right after deposition. To avoid this unwanted situation, no polymer layer was used but instead the devices were annealed right before measurement.

It was found that changing the stoichiometry towards more S-rich character gives rise to p-type doping and eventually the behaviour shifts from semiconductive to metallic. This general trend can be explained by a shift of the Fermi level from somewhere halfway in the band gap towards and into the valence band. The conductance of the device at zero gate voltage was increased by almost three orders of magnitude from $8.4 * 10^{-8}$ S for almost intrinsic PbS to $7.2 * 10^{-5}$ S for the most metallic-like device.

The transition to metallic behaviour is estimated to occur by the addition of 172 sulfide ions per PbS quantum dot of diameter 3.5 nm. More measurements on the ordering of the QDs in the thin film are needed to improve the uncertainty in this number. Estimating the original QD composition to be $Pb_{450}S_{410}$, this amount corresponds to a S/Pb ratio of 1.3. This result is in line with predictions based on DFT calculations reported in literature, according to which the transition takes place at a S/Pb ratio between 1.08 and 1.45.

CQDs are very promising for future use in optoelectronic devices because of the tunability of the band gap and low-cost production techniques. However, the mobility of the charge carriers and the ability to controllably dope the CQDs have to be improved before they can have a technological interest. The most basic component of a solar cells and an LED is a p-n junction, therefore it is essential to have both n-type and p-type semiconductors. As of July 2016, the record efficiency of CQD-based solar cells is 11.3% [27], a value which can be further increased by having heavier doping and more control over doping to optimize the junctions.

Acknowledgements

First of all, I would like to thank Daniel very much for his big support during the project. Thank you for training me in the lab and taking time for my many questions and doubts, and explaining matters clearly.

I am also very grateful to Maria, for setting me at ease when I was worried and for giving advice about the direction of the project and the report.

I also want to thank Musty, for helping me with the plotting software and for the nice conversations we had in the office.

Finally, I would like to thank all the people from the Photophysics and Opto-Electronics group. I really enjoyed the nice atmosphere.

References

[1] D. V. Talapin, J.-S. Lee, M. V. Kovalenko and E. V. Shevchenko, “Prospects of Colloidal Nanocrystals for Electronic and Optoelectronic Applications,” *Chemical Reviews,* vol. 110, no. 1, pp. 389-458, 2010.

[2] J. J. Shiang, A. V. Kadavanich, R. K. Grubbs and A. P. Alivisatos, “Symmetry of Annealed Wurtzite CdSe Nanocrystals: Assignment to the C3v Point Group,” *Journal of Physical Chemistry,* vol. 99, no. 48, pp. 17417-17422, 1995.

[3] S. Baskoutas and A. Terzis, “Size-dependent band gap of colloidal quantum dots,” *Journal of Applied Physics,* vol. 99, no. 1, pp. 013708-1 - 120708-4, 2006.

[4] L. Brus, “Electronic Wave Functions in Semiconductor Clusters: Experiment and Theory,” *Journal of Physical Chemistry,* vol. 90, no. 12, pp. 2555-2560, 1986.

[5] D. J. Norris, A. L. Efros and S. C. Erwin, “Doped Nanocrystals,” *Science,* vol. 319, no. 5871, pp. 1776-1779, 2008.

[6] A. Stavrinadis and G. Konstantatos, “Strategies for the Controlled Electronic Doping of Colloidal Quantum Dot Solids,” *ChemPhysChem,* vol. 17, no. 5, pp. 632-644, 2016.

[7] P. Atkins and J. de Paula, Physical Chemistry, Oxford: Oxford University Press, 2010.

[8] A. L. Efros and M. Rosen, “The Electronic Structure of Semiconductor Nanocrystals,” *Annual Review of Materials Science,* vol. 30, pp. 475-521, 2000.

[9] S. Neeleshwar, C. L. Chen, C. B. Tsai, Y. Y. Chen, C. C. Chen, S. G. Shyu and M. S. Seehra, “Size-dependent properties of CdSe quantum dots,” *Physical Review B,* vol. 71, no. 20, pp. 201307-1 - 201307-4, 2005.

[10] W. Shockley and H. J. Queisser, “Detailed Balance Limit of Efficiency of p-n Junction Solar Cells,” *Journal of Applied Physics,* vol. 32, no. 3, pp. 510-519, 1961.

[11] M. Yuan, M. Liu and H. Sargent, “Colloidal quantum dot solids for solution-processed solar cells,” *Nature Energy,* vol. 1, pp. 16016: 1-8, 2016.

[12] M. Bruchez Jr., M. Moronne, P. Gin, S. Weiss and A. P. Alivisatos, “Semiconductor Nanocrystals as Fluorescent Biological Labels,” *Science,* vol. 281, no. 5385, pp. 2013-2016, 1998.

[13] C. Donegá, P. Liljeroth and D. Vanmaekelbergh, “Physicochemical Evaluation of the Hot-InjectionMethod, a Synthesis Route for MonodisperseNanocrystals,” *Small ,* vol. 1, no. 12, pp. 1152-1162, 2005.

[14] D. Zherebetskyy, M. Scheele, Y. Zhang, N. Bronstein, C. Thompson, D. Britt, M. Salmeron, P. Alivisatos and L. Wang, "Hydroxylation of the surface of PbS nanocrystals passivated with oleic acid," *Science,* vol. 344, no. 6190, pp. 1380-1384, 2014.

[15] C. R. Kagan and C. B. Murray, "Charge transport in strongly coupled quantum dot solids," *Nature nanotechnology,* vol. 10, no. 12, pp. 1013-1026, 2015.

[16] E. Lifshitz, M. Bashouti, V. Kloper, A. Kigel, M. S. Eisen and S. Berger, "Synthesis and Characterization of PbSe Quantum Wires, Multipods, Quantum Rods, and Cubes," *Nano Letters,* vol. 3, no. 6, pp. 857-862, 2003.

[17] P. Guyot-Sionnest, "Electrical Transport in Colloidal Quantum Dot Films," *The Journal of Physical Chemistry Letters,* vol. 3, no. 9, pp. 1169-1175, 2012.

[18] D. Kim, D.-H. Kim, J.-H. Lee and J. C. Grossman, "Impact of Stoichiometry on the Electronic Structure of PbS Quantum Dots," *Physical Review Letters,* vol. 110, no. 19, pp. 196802 1-5, 2013.

[19] S. Z. Bisri, C. Piliego, J. Gao and M. A. Loi, "Outlook and Emerging Semiconcucting Materials for Ambipolar Transistors," *Advanced Materials,* vol. 26, no. 8, pp. 1176-1199, 2013.

[20] J. Zaumseil and H. Sirringhaus, "Electron and Ambipolar Transport in Organic Field-Effect Transistors," *Chemical Reviews,* vol. 107, no. 4, pp. 1296-1323, 2007.

[21] I. Moreels, K. Lambert, D. Smeets, D. De muynck, T. Nollet, J. C. Martins, F. Vanhaecke, A. Vantomme, C. Delerue, G. Allan and Z. Henst, "Size-Dependent Optical Properties of Colloidal PbS Quantum Dots," *ACS Nano,* vol. 3, no. 10, pp. 3023-3030, 2009.

[22] J. e. a. Tang, "Quantum Dot Photovoltaics in the Extreme Quantum Confinement Regime: The Surface-Chemical Origins of Exceptional Air- and Light-Stability," *ACS Nano,* vol. 4, no. 2, pp. 869-878, 2010.

[23] M. Tyona, "A theoritical study on spin coating technique," *Advances in Materials Research,* vol. 2, no. 4, pp. 195-208, 2013.

[24] K. S. Leschkies, M. S. Kang, E. S. Aydil and D. J. Norris, "Influence of Atmospheric Gases on the Electrical Properties of PbSe Quantum-Dot Films," *Journal of Physical Chemistry,* vol. 114, no. 21, pp. 9988-9996, 2010.

[25] D. Balazs, M. Nugraha, S. Bisri, M. Sytnyk, W. Heiss and M. Loi, "Reducing charge trapping in PbS colloidal quantum dot solids," *Applied Physics Letters,* vol. 104, pp. 112104-1 - 112104-4, 2014.

[26] A. V. Kurzin, A. N. Evdokimov, V. S. Golikov and O. S. Pavlova, "Solubility of Sodium Sulfide in Alcohols," *Journal of Chemical and Engineering Data,* vol. 55, no. 9, pp. 4080-4081, 2010.

[27] N. R. E. Laboratory, "Best Research-Cell efficiencies," [Online]. Available: http://www.nrel.gov/ncpv/images/efficiency_chart.jpg. [Accessed 05 07 2016].